AIAA 01-0735
Multiple Mode Actuation of a Turbulent Jet

LaTunia G. Pack
NASA Langley Research Center
Hampton, VA

Avi Seifert
Tel-Aviv University, Ramat-Aviv, Israel
and
ICASE, NASA Langley Research Center
Hampton, VA

39th Aerospace Sciences Meeting & Exhibit
8–11 January 2001
Reno, Nevada

Multiple Mode Actuation of a Turbulent Jet

LaTunia G. Pack* and Avi Seifert**
Flow Physics and Control Branch
NASA Langley Research Center, Hampton, VA 23681

Abstract

The effects of multiple mode periodic excitation on the evolution of a circular turbulent jet were studied experimentally. A short, wide-angle diffuser was attached to the jet exit. Streamwise and cross-stream excitations were introduced at the junction between the jet exit and the diffuser inlet on opposing sides of the jet. The introduction of high amplitude, periodic excitation in the streamwise direction enhances the mixing and promotes attachment of the jet shear-layer to the diffuser wall. Cross-stream excitation applied over a fraction of the jet circumference can deflect the jet away from the excitation slot. The two modes of excitation were combined using identical frequencies and varying the relative phase between the two actuators in search of an optimal response. It is shown that, for low and moderate periodic momentum input levels, the jet deflection angles depend strongly on the relative phase between the two actuators. Optimum performance is achieved when the phase difference is $\pi \pm \pi/6$. The lower effectiveness of the equal phase excitation is attributed to the generation of an azimuthally symmetric mode that does not produce the required non-axisymmetric vectoring. For high excitation levels, identical phase becomes more effective, while phase sensitivity decreases. An important finding was that with proper phase tuning, two unsteady actuators can be combined to obtain a non-linear response greater than the superposition of the individual effects.

Nomenclature

A_{jet}	jet cross-section area, πr^2
A_{slot}	active slot area, $\pi h(2r+h)/4$
$<c_\mu>$	periodic momentum coefficient, $J'/(\rho A_{jet} U_e^2)$
D	jet diameter
F^+	reduced frequency, fL/U_e
f	excitation frequency [Hz]
h	slot width or height
J'	periodic momentum at slot exit, $\rho A_{slot} u'^2_{slot}$
k	constant for kilo, 1000
L	distance from jet exit to diffuser exit, measured along diffuser wall
m	mode
p	pressure
r	jet radius, D/2
Re_D	Reynolds number based on diameter, $U_e D/\nu$
RMS	root mean square of fluctuating value
S_{tD}	Strouhal number based on jet diameter, fD/U_e
$S_{t\theta}$	Strouhal number based on momentum thickness, $f\theta/U_e$
T	period of excitation
t	time
U	jet mean streamwise velocity
u'	root mean square of the streamwise velocity fluctuations
V	jet mean cross-stream velocity
x	axial direction, x=0 at jet exit and diffuser inlet
y	vertical direction, y=0 at jet centerline
z	horizontal direction, z=0 at jet centerline
δ	jet deflection angle, [deg]
ϕ	phase angle between two actuators
φ	diffuser half-angle
θ	jet two-dimensional shear-layer momentum thickness
ρ	density
ν	kinematic viscosity

Subscripts

b	baseline
d	de-rectified
e	conditions at jet exit
max	maximum
pl	plane
pr	profile
R	cross-stream excitation
slot	condition at slot exit
X	streamwise excitation
(X+R)	combined excitation
0.5	location where U/U_e=0.5

* Research engineer, Flow Physics and Control Branch, member AIAA.
** Senior lecturer, Dep. of Fluid Mech. & Heat Transfer, Faculty of engineering, Tel-Aviv University, Ramat-Aviv 69978, ISRAEL. Also: ICASE, NASA Langley Research Center, visiting scientist. Senior member, AIAA.

5hp 5-hole probe

1. Introduction

Modification of the evolution and characteristics of turbulent jets is of great practical importance. Such modification can lead to noise generation or cancellation, mixing enhancement or attenuation, and thrust vectoring. The relevance of coherent structures to the evolution and control of turbulent jets is widely accepted[1] as is the relationship to stability theory[2,3], even though the background flow is turbulent and the amplitudes are finite. It was envisioned[2] and later demonstrated[4,5] that non-linear interaction between different unsteady modes could lead to a mean flow distortion in the form of enhanced mixing or vectoring. However, the expected modification is dependent upon the magnitude of the coupling between the linear modes that tend to saturate. It was demonstrated experimentally[6,7] and numerically[8] that the presence of a confinement at the jet exit promotes the generation of coherent structures. These in turn interact with the jet flow and wall to locally reduce the static pressure and pull the jet flow towards the wall. High amplitude periodic excitation can either pull the jet towards the excited shear-layer or push it away[7,9], depending on the relative direction between the excitation and the jet stream. When introduced into opposite shear-layers, each mode could deflect the jet flow in the same direction. The next logical step would be to combine the two modes in order to increase the overall effect. In doing so, additional parameters come into play, such as the relative frequency and amplitude as well as the phase lag between the two actuators.

Under current investigation are the effects of combining the two modes while operating at the same frequency and varying the relative phase. In most cases, the amplitudes were tuned such that each actuator generated a similar jet modification when operated alone.

Section 2 provides a description of the experiment, and Section 3 is an overview of the effect seen when combining the streamwise and cross-stream excitation at different phases. Section 4 provides a possible explanation for the observed effect, and the conclusions are provided in Section 5.

2. Experiment Set-up

Figures 1a and 1b show schematics of the jet front and side views. The jet exit diameter was 39 mm. A 1mm wide slot, divided into four equal segments surrounded the jet exit as shown in Figure 1a. Each segment of the slot was connected to a cavity, allowing independent excitation of every 90 deg of the jet circumference. Streamwise excitation was introduced through the 90 deg segment of the slot surrounding the right side of the jet (positive z, see Fig. 1a). Cross-stream excitation was introduced through the 90 deg segment of the slot surrounding the left side of the jet (looking into the jet, negative z, Fig. 1a). Trip grit (#36) was evenly distributed on an adhesive strip 12.7mm wide, and the strip bonded inside the jet pipe, 200 mm upstream of the jet exit (Fig. 1b), to ensure that the flow at the jet exit was turbulent over the velocity range of interest (8 m/s - 18 m/s). All the data presented in this paper are for a jet exit velocity of 12 m/s, resulting in a Reynolds number based on a jet exit diameter of 31,000.

A short, wide-angle diffuser was attached to the exit of the jet. The diffuser half-angle, φ, was 30 deg and the length, L, was 1.85D. The diffuser could have been significantly shorter and still effective[7]. The inlet geometry of the diffuser was different on each side of the jet exit to allow periodic excitation to be introduced in the streamwise direction on one side of the jet and in the cross-stream direction on the other side. Excitation in the streamwise direction is referred to as the X-excitation, and excitation in the cross-stream direction is referred to as the R-excitation.

Two zero-mass-flux piezo-electric actuators, each with a resonant frequency of approximately 700 Hz, were used to generate the periodic excitation. The velocity fluctuations, u', exiting the slot were measured using a hot-wire positioned at the slot exit. Since hot-wires cannot sense flow direction, the velocities obtained at the slot exit, in the absence of jet flow, were de-rectified[10]. The maximum RMS of the velocity fluctuations, u'_{max}, when operated at 700 Hz using X-excitation, was about 18 m/s. The value of u'_{max} was about 10% lower for the R-excitation. Variations in the jet exit velocity or the presence of a diffuser changed the slot u' by less than 5%. Each slot was calibrated at three circumferential locations separated by 22.5 deg, and the resulting values of u' did not deviate by more than 6% for u' values above 3 m/s.

The hot-wire data were acquired using an eight channel simultaneous sample, 16-bit analog-to-digital converter. The sampling rate was 12.8 kHz, and the input was low pass filtered at 5 kHz. The actuators were driven sinusoidally using a two-channel variable-phase function generator combined with a multi-channel power amplifier. The phase resolution of the function generator was 1 deg. Dynamic pressure transducers were installed in the actuator cavities (Fig. 1a) to monitor the excitation level throughout the experiment. Mean pressures from a 5-hole probe were measured with 10 torr capacitive differential pressure transducers and a 22 bit voltmeter coupled with a relay multiplexer.

A 300 mW argon ion laser generated a light sheet for the flow visualization images acquired to characterize the jet flow field. The jet was seeded using a theatrical smoke generator placed upstream of the fan. Eight-bit flow-field images were acquired using a digital camera and a digital frame grabber card. The shutter speed was set to 0.008 seconds, and the images presented are an average of at least 50 instantaneous images.

The velocities measured with the hot-wire are accurate to within ±2%. The hot-wire position (x, y, or z) is accurate to within ±0.04 mm, Re_D is accurate to within ±3%, the periodic momentum coefficient, $<c_\mu>$, is accurate to within ±15%, and the jet deflection estimates are accurate to within ±1.5 deg when calculated from a single hot-wire profile measured at the jet center plane.

3. Discussion of Results

3.1 Overview of Jet Modes

Hot-wire surveys and smoke flow visualization images of the jet were acquired at a cross-stream plane of x/D=2.5 and $Re_D=3.1\times10^4$. Streamwise and cross-stream excitation levels were chosen to produce a jet deflection between 2.5° and 3.0° using either excitation alone. Figure 2 shows the flow visualization images and contours of the mean velocities for the various excitation types used. The baseline, $<c_\mu>_X = <c_\mu>_R = 0$, flow field images and velocity contours presented in Figures 2a and 2f are circular as expected. Slight deviations from a circular pattern are believed to be due to the presence of different slot configurations affecting the jet boundary conditions. Cross-stream excitation with $F^+=4.2$ and $<c_\mu>_R=1.5\%$ on the left-hand side of the jet causes a deflection of δ_{pl} ~3.0° towards the right-hand side as shown in Figures 2b and 2g. A more detailed description of the method used for determining the jet deflection angle is presented in Section 3.2. Figures 2b and 2g indicate that cross-stream excitation pushes the jet towards the right side causing the jet to contract in the z direction and expand in the y direction with respect to the baseline. Streamwise excitation with $F^+=4.2$ and $<c_\mu>_X=0.58\%$ deflects the jet by δ_{pl} ~2.6° towards the excited shear-layer (right side) as shown in Figures 2c and 2h. Note that the regions where the smoke overlaps the diffuser wall have been removed from Figures 2c and 2e for clarity. The jet spreads more on the side of the excited shear-layer. Similar results for slightly different excitation momentum levels were presented in Reference 7.

In this paper, the effect of combining the cross-stream and streamwise excitations on opposing sides of the jet is examined. The streamwise and cross-stream excitations are combined in-phase (ø=0°) in Figures 2d and 2i. The velocity contours in Figure 2i indicate that the overall effect is similar to that seen when exciting the flow using the R-excitation alone (Fig. 2g). However, the U contours for the ø=0° excitation are slightly more spread in the z direction and less in the y direction than the R-excitation U contours (Fig. 2g). The jet deflection resulting from the in-phase combination of the two excitations is δ_{pl}~6°, about the same as the sum of the individual effects. This type of excitation allows the jet to be deflected efficiently with only moderate spreading. The out-of-phase (ø=180°), combination of R- and X-excitation results in a jet deflection of δ_{pl} ~7°, more than the sum of the deflections obtained when exciting the jet with each separately. The velocity contours and smoke flow visualization images of Figures 2e and 2j indicate that the effect of the ø=180° excitation is similar to that of the ø=0° excitation on the left side of the jet. The effect of streamwise excitation is more evident in the ø=180° contours on the right-hand side, similar to the effect of the X-excitation alone (Fig. 2h). The observed effect of the relative phase between the two actuators (even at high Strouhal numbers) indicates that further study is required.

3.2 Determination of Jet Deflection Angles

The method of determining the jet deflection angle was described in detail in Reference 7 and is included here for completeness. Deflection angles based on hot-wire data were calculated in the following manner. The total streamwise linear momentum, M, at a given vertical location, y/D, was computed using

$$M_j = \int U^2 dz \qquad \text{(Eq. 1a)}$$

where U is the jet mean velocity at a given spanwise, z, position in the profile, and j is an index denoting the increment in the vertical, y, direction. Note density has been neglected in Eq. 1a because of incompressibility and the eventual cancellation of the term that occurs when computing jet deflection angles. The data were integrated over the range of the hot-wire calibration velocities. The center of linear momentum of the jet at a given vertical location, y/D, was determined by computing the ratio of the moment of momentum to the momentum in the form

$$z_{c,j} = \frac{\int U^2 z dz}{\int U^2 dz} \qquad \text{(Eq. 1b).}$$

The deflection angle based on one profile, δ_{pr}, measured at y/D=0 is defined as,

$$\delta_{pr} = \tan^{-1}\left(\frac{z_{c,pr}}{x}\right) \qquad \text{(Eq. 2)},$$

where x is the distance from the jet exit to the measuring station. Complete cross-sectional planes of hot-wire data were also used, in the following manner, to evaluate the jet deflection angle. The center of linear momentum of the jet at a given cross-stream location, x/D, was determined by computing a weighted average of the centers of momentum for all the profiles acquired in the plane using momentum as the weight function in the form

$$z_{c,pl} = \frac{\sum_j M_j z_{c,j}}{\sum_j M_j} \qquad \text{(Eq. 3)}.$$

The deflection angle based on a whole cross-sectional plane, δ_{pl}, was determined by assuming that the jet began deflecting at x/D=0.0 and computing the angle between z=0 and $z_{c,pl}$ using

$$\delta_{pl} = \tan^{-1}\left(\frac{z_{c,pl}}{x}\right) \qquad \text{(Eq. 4)}.$$

A comparison of the jet deflection angles based on a single profile, δ_{pr}, measured at y=0 to the jet deflection angles based on profiles that were acquired over the entire cross-section, δ_{pl}, at x/D=2.5, is presented in Figure 3. The jet deflection estimates from a single velocity profile, δ_{pr}, are about 1° higher than those computed using the data from the entire jet cross-sectional plane, δ_{pl}. The highest deviation seen is for the X-excitation, due to a larger deviation from circular symmetry for the X-excitation as shown in Figures 2c and 2h.

A limited number of three-component velocity profiles were acquired using a 5-hole probe[11]. The jet deflection angles from the five-hole probe data were computed using the local flow angle

$$\delta_{5,i} = \tan^{-1}\left(V_i/U_i\right) \qquad \text{(Eq. 5)}.$$

This was inserted into the z component of the linear momentum equation applied to a control volume in the form

$$\delta_{5hp} = \frac{\sum_i U_i^2 \delta_{5,i}}{\sum_i U_i^2} \qquad \text{(Eq. 6)},$$

where i is an index in the horizontal direction, z. Data acquired where the local velocity, U, was greater than $0.125U_e$ were included in the average. Figure 4 shows a comparison of jet deflection angles based on 5-hole probe velocity profiles at y=0 with jet deflection angles based on hot-wire profiles acquired at the same location. For these data, F^+=4.2, $\langle c_\mu \rangle_R$=0.89%, and $\langle c_\mu \rangle_X$=0.2%. The agreement between the 5-hole probe and hot-wire data is within ±0.5°, better than the results of the comparison between jet deflections based on a single profile and jet deflections based on a series of profiles over the entire cross-section. The agreement between δ_{pr} and δ_{5hp} provides added validity to the deflection estimate approach. The velocity profiles used for computing 5-hole probe and hot-wire deflection angles are presented in Figure 5. There is very good agreement between the hot-wire mean velocity U and the 5-hole probe streamwise velocity component, where larger deviations could be seen at the jet shear-layers. This is especially true for the right side of the jet due to non-vanishing cross-stream velocity, V, when using the ø=π excitation. The V profiles for the baseline are slightly biased to the positive direction, indicative of a possible slight misalignment of the probe to the streamwise direction. The effect of the jet deflection is clearly seen as the entire V profile for the (X+R) excitation is shifted to obtain positive values of V, especially on the right hand side of the jet. The remainder of the data, beginning with Figure 6, is based on hot-wire measurements.

3.3 Optimal Deflection Angle

As shown in Reference 7, periodic excitation combined with a short, wide-angle diffuser can be used to effectively deflect a jet. Deflection angles using either R- or X-excitation, applied to opposing shear-layers, exceed 8° when using $\langle c_\mu \rangle$ ~5%, as shown in Figure 6. To enhance the effect (generate greater deflection angles), the two modes of excitation were combined. The deflection angles produced by the optimal combination of the two excitations are also presented in Figure 6. The $\langle c_\mu \rangle_{(X+R)}$ values are a sum of the $\langle c_\mu \rangle$ values generated by each actuator when operated alone. Much higher deflection angles can be obtained when the two modes of excitation are operated simultaneously with the appropriate phase shift. The details of the optimal phase will be discussed later. Figure 7 presents a comparison of jet deflection angles generated by optimally phased (X+R) excitation with jet deflection angles computed by adding the deflection angles from the individual X- and R-excitations. Optimally phased excitation produces jet deflection angles that are higher than the sum of the individual jet deflection angles produced by the X- and R-excitations. The relative increase in jet deflection angles is higher for the lower $\langle c_\mu \rangle$ levels, but this finding cannot be easily seen in the scales of Figure 7.

Baseline and controlled jet velocity profiles using F^+=4.2, $\langle c_\mu \rangle_X$=0.06%, and $\langle c_\mu \rangle_R$=0.84% are presented

in Figure 8a. X-excitation primarily affects the right side (positive z) of the jet producing a jet deflection of 1.51°. R-excitation mainly affects the left side (negative z) of the jet, producing a jet deflection of 2.0°. In-phase, ø=0°, excitation appears to diminish the effect of the X-excitation, producing a jet deflection of only 2.4°. The ø=180° excitation produces a jet deflection of 4.3°. This deflection is more than the sum of the deflection angles, $\delta_{pr,X}$~1.51° and $\delta_{pr,R}$~2.0°, produced by the X-excitation and R-excitation alone.

The sensitivity of the jet deflection angle to the relative phase between the X- and R-excitations is presented in Figure 8b for relatively low values of $<c_\mu>$. The jet deflection angles have all been referenced to the sum of the individual deflection angles, $\delta_X+\delta_R$. It is clearly demonstrated that ø=0° is not the optimal combination of the two excitation modes. The in-phase, ø=0°, combination of the two excitations leads to a reduction in the effectiveness of the combined excitation as compared to a linear superposition of the individual effects. Positive interaction (i.e., a deflection angle greater than the deflection angle produced by the two excitations operated independently) occurs only for phase angles greater than 90°. The jet deflection angles obtained for the $<c_\mu>$ levels presented in Figure 8b indicate that the optimum phase angle is $ø=\pi\pm\pi/6$. A comparison of the $<c_\mu>$ levels presented for the F^+=4.2 cases indicates that the ø sensitivity decreases with increasing $<c_\mu>$. A comparison of the two frequencies presented in Figure 8b indicates that the ø sensitivity at F^+=2.1 is greater than that at F^+=4.2 for the $<c_\mu>$ range examined.

Figure 8c presents jet velocity profiles at x/D=2.5 and y/D=0.0 for varying phase using (X+R) excitation with F^+=4.2, $<c_\mu>_X$=0.58%, and $<c_\mu>_R$=1.56%. The effect of increasing phase is mainly to enhance the jet spreading on the X-excited side of the jet. Profiles of u' (not shown) indicate that the velocity fluctuations increase on the R-excitation side with increasing phase, while they decrease on the X-excitation side, as a result of the enhanced spreading and reduced shear. From this point we shall concentrate on ø=0° and ø=180°, while noting that an optimal performance at low $<c_\mu>$ could be found at $ø=\pi\pm\pi/6$.

The effect of the relative phase between the X-and R-excitations over a wide range of $<c_\mu>_X$ and $<c_\mu>_R$ values, was quickly evaluated by placing two hot-wires, one in each shear layer of the jet, at x/D=2.5 and y/D=0.0. The hot-wires were placed at the z location in the shear-layer where U/U_e=0.5, $z_{0.5}$, of the baseline jet. These z locations were at the mid-point of the circumferential distance covered by the R-excitation and X-excitation actuators. Data were acquired with the actuators operating in-phase and 180° out of phase over a $<c_\mu>_X$ range of 0-5.06% and a $<c_\mu>_R$ range of 0-2.58%. The difference in velocity between the baseline and excited shear-layer was computed on both the R-excitation side and the X-excitation side of the jet. The two differences were multiplied by each other and negated to yield a positive quantity representative of the jet modification due to the excitation. This term, $-\Delta U_R \Delta U_X$, was selected since reducing U on the left side and increasing U on the right side is what would be expected when attempting to deflect the jet to the right. Contours of these results are shown in Figure 9a. If the slope of constant $-\Delta U_R \Delta U_X$ contour lines would be -45° then that would indicate that both modes contribute the same to the combined effect. It is evident that $<c_\mu>_X$ is more effective than $<c_\mu>_R$, regardless of ø. The slope approaches –45° only at the upper right corner of the ø=180° contours (Fig. 9b). At high $<c_\mu>$, the difference between the two phase angles is small, indicating a reduced ø sensitivity. At low $<c_\mu>$, combining the R-excitation and the X-excitation at ø=180° is more effective at deflecting the jet than the in-phase, ø=0°, combination of the two excitations. This is especially evident for low values of $<c_\mu>_X$ where increasing $<c_\mu>_R$ at ø=0° decreases the effectiveness of $<c_\mu>_X$.

The change in shear-layer velocity at $z_{0.5,b}$ on the R- and X-excitation sides of the jet due to varying $<c_\mu>_R$ between 0-2.58% is shown in Figures 9c and 9d for two values of $<c_\mu>_X$ (0.25% and 2.4%). Shear-layer results are given for the ϕ=0° and ϕ =180° combinations of (X+R) excitation. Regardless of $<c_\mu>_R$, the shear-layer excited by the R-excitation is insensitive to ø (Fig. 9c), while the shear-layer excited by the X-excitation is very sensitive to ϕ, (Fig. 9d). As $<c_\mu>_X$ increases from 0.25% to 2.4%, the ø sensitivity of the X-excited shear-layer decreases. At low $<c_\mu>_X$, ø=π is more effective, while at high $<c_\mu>_X$, ø=0° is more effective (Fig. 9d). The overall sensitivity to ø is reduced with increasing $<c_\mu>$.

3.4 Jet Flow Field Close to Source

The results presented thus far have focused on the effect of the R- and X-excitations at a single streamwise location, x/D=2.5. In this section, data closer to the excitation source and the jet exit were examined to determine if the global effects seen at x/D=2.5 represent flow behavior near the source and to learn more about the physical mechanism causing the observed results. The change in the center of momentum, z_c, with axial location is shown in Figure 10 for the in-phase and 180° out-of-phase combination of the X- and R-excitations using F^+=4.2, $<c_\mu>_X$=0.14%, and $<c_\mu>_R$=1.76%. The jet deflection angles produced by the R-excitation and X-excitation independently are

$\delta_{pr,R}$=4.4° and $\delta_{pr,X}$=3.2°. The ø=0° combination of the X- and R-excitation results in a deflection angle of 5.1°, and the ø=180° combination of the two excitations results in a deflection angle of 7.7°. These deflection angles were computed based on data measured at x/D=2.5. Deflection angles computed from data taken closer to the source are smaller due to the fact that the virtual origin of the jet is somewhat upstream of x/D=0.0. As shown in Figure 10, the virtual origin of the deflected jet is close to x/D=-0.25. The jet deflection angle can also be computed from the inverse tangent of the slopes of the curves in Figure 10. This approach yields jet deflection angles of 4.9° and 7.2° for ø=0° and ø=180°, respectively. These results are in good agreement with the jet deflection angles based on the shift in linear momentum measured at x/D=2.5 (5.1° and 7.7°, respectively).

The streamwise variation of the shear-layer location where the local velocity is 50% of the free-stream velocity, $z_{0.5}$, is shown in Figure 11 for the baseline, the in-phase (ø=0°) and 180° out-of-phase excitations used in Figure 10. The values of $z_{0.5}$ for the baseline jet are fairly constant, resulting in dz/dx~0 for both shear-layers. The in-phase (ø=0°) combination of the X- and R-excitations results in a vectoring of the jet on the left side as evidenced by the increase in slope (dz/dx=0.13) with respect to the baseline. However, on the right side of the jet, the ø=0° excitation does not modify the $z_{0.5}$ location of the jet significantly (dz/dx=0.03). The (X+R), ø=0° excited jet is contracted in this plane, based on the $z_{0.5}$ lines, as was also shown in the velocity contours of Figure 2i. The ø=180° combination of the X-and R-excitations causes the jet to be more effectively vectored towards the right resulting in dz/dx values of 0.15 and 0.10 on the left and right sides of the jet, respectively. The $z_{0.5}$ lines for the (X+R), ø=180° excited jet, clearly demonstrate the vectoring of the jet column. The distance between $z_{0.5}$/D,left and $z_{0.5}$/D,right is 0.95 for the baseline jet, 0.80 for the (X+R), ø=0° excited jet and 0.91 for the (X+R), ø=180° excited jet at x/D=2.5.

4. Physical Interpretation of Observations

The physical mechanism responsible for the changes seen when varying the phase between the two actuators used to control the jet could be explained by the variations in the resulting jet modes that are excited by the actuators. In Figures 12a and 12b the amplitude of u' at 700 Hz, corresponding to the planes that were measured at x/D=2.5 and discussed in Section 3.1 are examined. The amplitude distribution of the in-phase excitation is closer to being circular, this suggests that a higher level of the axisymmetric, m=0, mode of the jet may have been excited, even though the total energy at the excitation frequency is similar for both the in-phase and ø=180° combination of the X- and R-excitations. A Fourier decomposition of the excitation input around the jet exit indicates that higher levels of mode zero could have been generated when using (X+R) excitation with ø=0° to excite the jet.

Data at x/D=1.0 is examined to further explore the idea that the in-phase and out-of-phase combination of the X-and R-excitations excite different modal distributions of the jet. Mean and fluctuating streamwise velocity profiles at x/D=1.0, F^+=4.2, $\langle c_\mu \rangle_X$=0.14%, and $\langle c_\mu \rangle_R$=1.76% are presented in Figure 13a for the in-phase and ϕ=180° combination of the two excitations. The right side (X-excited) shear-layer spreads more when combining the X- and R-excitations, 180° out of phase, as was also indicated by the location of $z_{0.5}$ in Figure 11. The fluctuating velocity, u', profiles indicate that the in-phase combination of the (X+R) excitation is closer to being symmetric, i.e., more mode zero was indeed generated while the u' profile for the ø=π excitation combination is not symmetric.

Figure 13b and 13c present contour plots of phase locked velocity fluctuations, <u'>, for two cycles (2T) of the fundamental excitation frequency, corresponding to the data presented in Figure 13a. The phase coherence in the z direction is stronger for the ø=0° excitation as indicated by the relatively uniform and smooth distribution of the <u'> contours in the z direction. This also implies that m=0 is the dominant mode. A simplified analysis of mode shape shows that ø=0 excites more m=0 and 2 than ø=π. More of the odd modes (m=1,3,5, etc) will be excited at ø=π. Mode m=0 will counteract the desired jet modification because it is inherently symmetric. A similar observation can be found in Figure 20 of Ref. 12 that also resulted in a smaller jet modification that was attributed to the presence of a significant level of mode zero.

Amplitude and phase distributions from the data presented in Figures 13a through 13c are presented in Figure 13d. The measured amplitude and phase distributions on the left side of the jet resemble the theoretically predicted m=0 and m=1 mode shapes. It is noted that the amplitudes are high and the problem is non-linear since the mean flow was modified. For ø=0°, the amplitude and phase distributions are much more symmetric than for ø=180°, i.e., there is a stronger contribution from mode zero for ø=0°. The ratio between the peak amplitude and the amplitude at the jet core (z~0) is higher for ø=0°, which is in agreement with the trend shown in Figures 9c and 9d of Reference 4 for the amplitude distributions of these modes in excited free jets. Loss of phase coherence was

observed on the X-excited shear-layer as well as over the entire jet when using X-excitation alone, while the effect of the R-excitation is of a more global nature[7]. A sign of such a loss of phase coherence could be seen on the positive z side of the (X+R) excited jet when ø=180° (Fig. 13d). This is an indication that the effect of the X-excitation on the jet persists when exciting the jet with the two actuators 180° out-of-phase.

5. Conclusions

Two actuators placed on opposite sides of a circular jet with a short, wide-angle diffuser attached at the jet exit, were activated simultaneously to control the jet deflection angles. One actuator slot covered a $\pi/4$ segment at the right side shear-layer and was pointed in the stream-wise direction. A second actuator slot, that also covered a $\pi/4$ segment, was placed in the opposite shear-layer and generated cross-stream excitation. When operated alone, each actuator was capable of deflecting the jet to the right side. The effectiveness of the streamwise excitation was greater than that of the cross-stream excitation. However, the two actuators were operated together at the same frequency in an attempt to increase the deflection angles and to search for a positive interaction that might lead to effects stronger than the effects expected from a linear superposition of the individual effects. It was demonstrated that with proper phase combinations of the two zero-mass-flux actuators, it is possible to obtain deflection angles higher than the sum of the effects of each actuator when operating individually. At low to medium periodic momentum input levels, a phase shift of $\pi \pm \pi/6$ was found to provide an optimum response. At large excitation levels, where the phase sensitivity was reduced, the absence of phase shift provided an optimum response. To understand the reason for the phase sensitivity, the jet flow field close to the excitation source (x/D=1.0) was studied. The reason for the differences in the jet modification due to variations of the relative phase of the excitation generated by the two actuators is assumed to be connected to an enhanced level of mode zero excitation that is generated when the two actuators are operated in-phase. A mode zero type of disturbance counteracts the required jet modification, i.e. deflection.

The practical aspect of these findings is that it would be possible to combine several actuators of modest control authority and generate a strong global effect that could be greater than the linear combination of the individual effects.

Acknowledgement

The authors would like to thank NASA Langley Flow Physics and Control Branch members Steve Wilkinson, Ponnampalam Balakumar, George Beeler, Anthony Washburn, Mike Walsh and William Sellers for their support.

References

1) Crow, S. C. and Champagne, F. H., "Orderly Structure in Jet Turbulence", *Journal of Fluid Mechancis*, Vol. 48, part 3, 1971, pp. 547-591.
2) Michalke, A., "Survey on Jet Instability Theory", *Progress in Aerospace Science*, Vol. 21, 1984, pp. 159-199.
3) Gaster, M., Kit, E., and Wygnanski, I., "Large-Scale Structures in a Forced Turbulent Mixing Layer", *Journal of Fluid Mechanics*, Vol. 150, 1985, pp. 23-39.
4) Cohen, J. and Wygnanski, I., " The Evolution of Instabilities in the Axisymmetric Jet. Part 1. The Linear Growth of Disturbances Near the Nozzle", *Journal of Fluid Mechanics*, Vol. 176, 1987, pp. 191-219.
5) Wygnanski, I. and Peterson, R. A., "Coherent Motion in Excited Free Shear Flows", AIAA paper 85-0539, March 1985.
6) Alvi, F. S., Strykowski, P. J., Krothapalli, A., and Forliti, D. J., "Vectoring Thrust in Mulitaxes using Confined Shear Layers", *Journal of Fluid Engineering*, Vol. 122, 2000, pp. 3-13.
7) Pack, L.G. and Seifert, A., "Periodic Excitation for Jet Vectoring and Enhanced Spreading", AIAA paper 99-0672, Jan. 1999. Also: *Journal of Aircraft*, May 2001, to appear.
8) Grinstein, F.F. and DeVore, C.R., "Entrainment and Thrust Vector Control with Countercurrent Rectangular Jets", AIAA paper 99-00165, Jan. 1999.
9) Smith, B. L., and Glezer, A., "Vectoring and Small-Scale Motions Effected in Free Shear Flows Using Synthetic Jet Actuators", AIAA paper 97-0213, Jan. 1997.
10) Seifert, A. and Pack, L.G., "Oscillatory Control of Separation at High Reynolds Numbers", *AIAA Journal*, Vol. 37, No. 9, September 1999, pp. 1062-1071.
11) Kinser. E. and Rediniotis, O.K., " Development of a Nearly-Omni-Directional, Three-Component Velocity Measurement Pressure Probe", AIAA paper 96-0037, 1996.
12) Parek, D. E., Kibens, V., Glezer, A., Wiltse, J. M., and Smith, D. M., "Innovative Jet Flow Control: Mixing Enhancement Experiment", AIAA paper 96-0308, Jan. 1996.

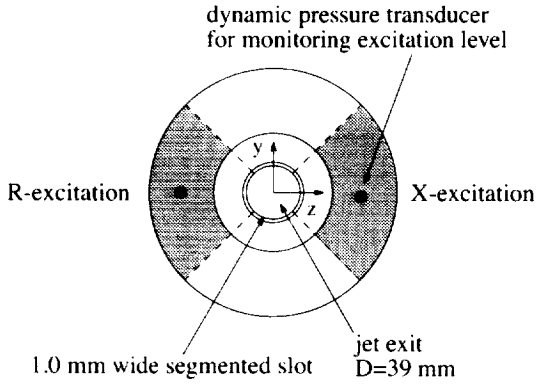

(a) front view

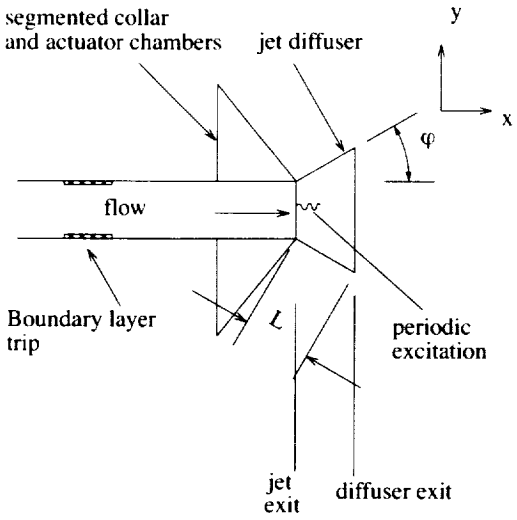

(b) side view

Figure 1 a-b: Schematic of the jet.

a: baseline jet

b: R-excited jet

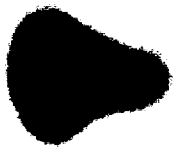

c: X-excited jet

d: X+R, ø=0° excited jet

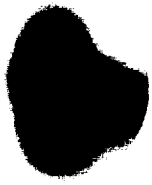

e: X+R, ø=180° excited jet

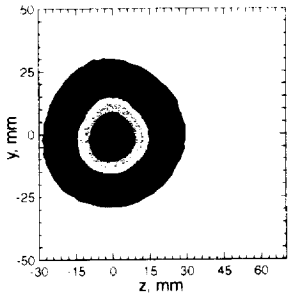

f: baseline jet

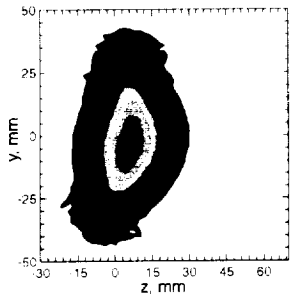

g: R-excited jet

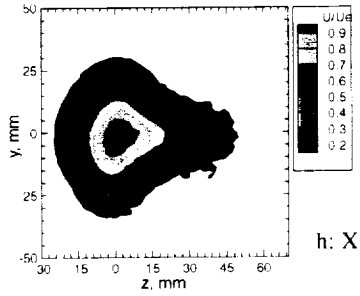

h: X-excited jet

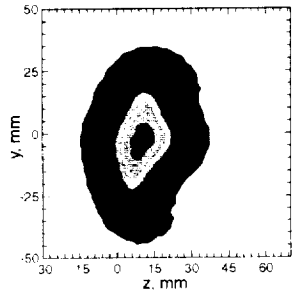

i: X+R, ø=0° excited jet

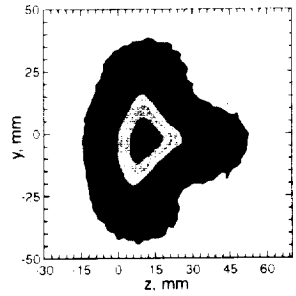

j: X+R, ø=180° excited jet

Figure 2a-j: Smoke flow visualization images (left column) and mean velocity contours (right column) at Re_D=3.1x10^4, x/D=2.5, U^+=4.2 $<c_\mu>_X$=0.58%, and $<c_\mu>_R$=1.5%.

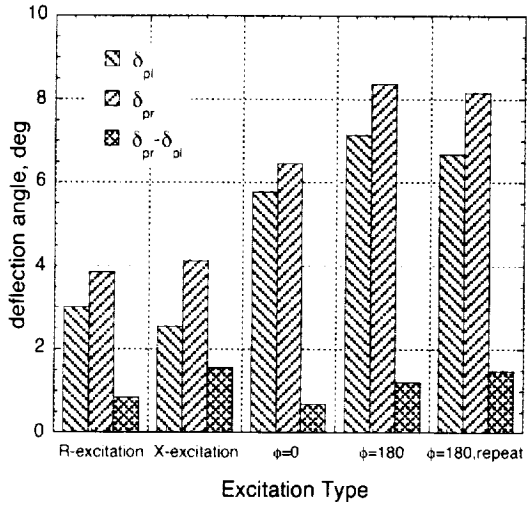

Figure 3: A comparison of δ_{pr} and δ_{pl} at x/D=2.5, Re_D=3.1x10⁴, F^+=4.2, $<c_\mu>_X$=0.58%, and $<c_\mu>_R$=1.5%.

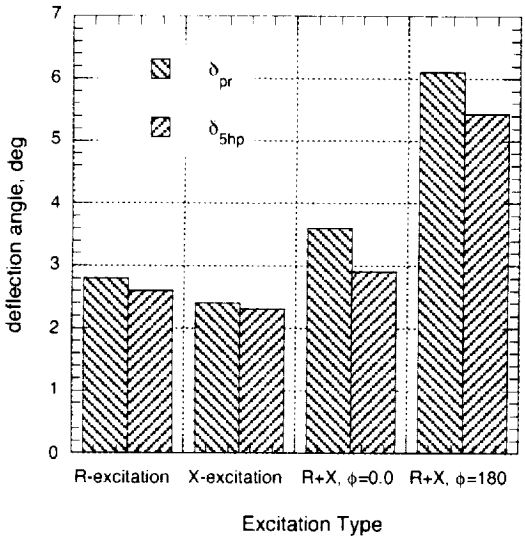

Figure 4: Comparison of jet deflection angles based on the center of momentum with jet deflection angles based on 5-hole probe data. F^+=4.2, $<c_\mu>_X$=0.2%, $<c_\mu>_R$=0.89%, x/D=2.5, and Re_D=3.1x10⁴.

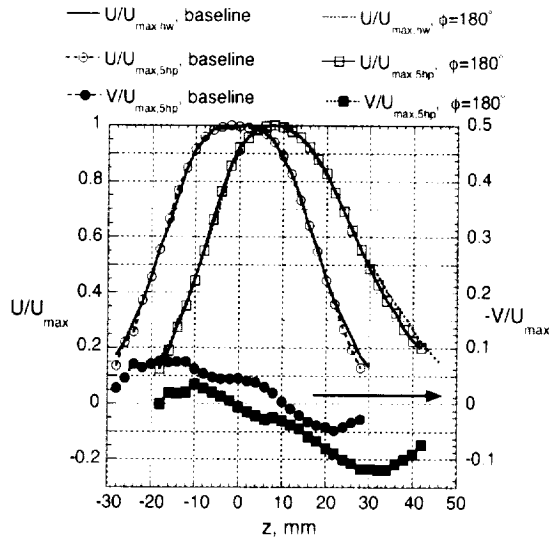

Figure 5: Baseline and controlled jet hot-wire and 5-hole probe velocity profiles at x/D=2.5 and Re_D=3.1x10⁴. F^+=4.2, $<c_\mu>_X$=0.2% and $<c_\mu>_R$=0.89% when control applied.

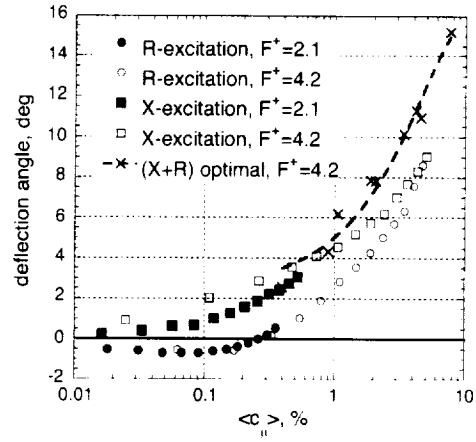

Figure 6: Jet deflection angles at x/D=2.5, Re_D=3.1x10⁴.

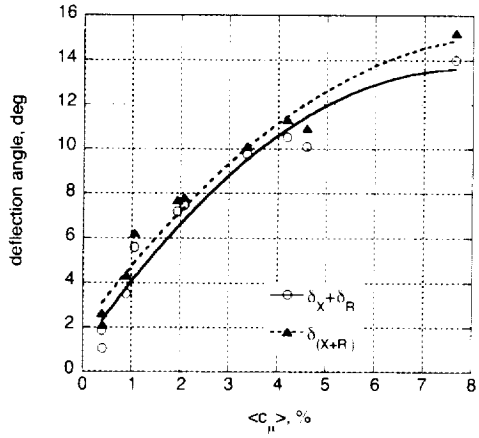

Figure 7: Comparison of the sum of the individual excitations and the properly phased (X+R) excitation, δ_{pr} presented.

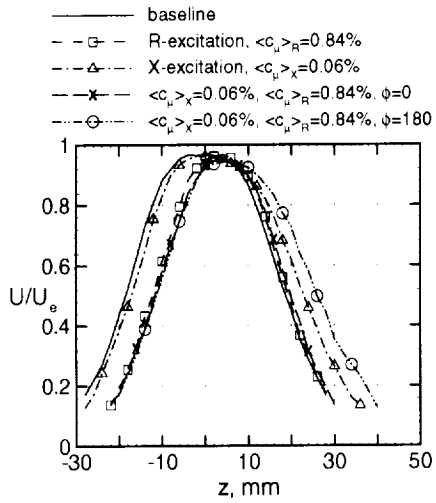

Figure 8a: Hot-wire mean velocity profiles at x/D=2.5, $Re_D=3.1x10^4$.

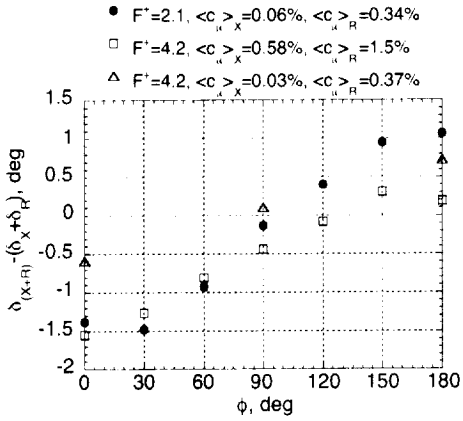

Figure 8b: Dependence of jet deflection angles on phase angle between X- and R-excitation, δ_{pr} presented.

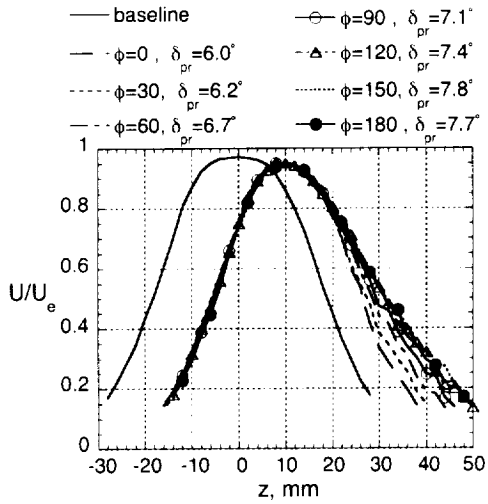

Figure 8c: Hot-wire mean velocity profiles at x/D=2.5, $Re_D=3.1x10^4$, ø varied, $<c_\mu>_X=0.58\%$ and $<c_\mu>_R=1.56\%$.

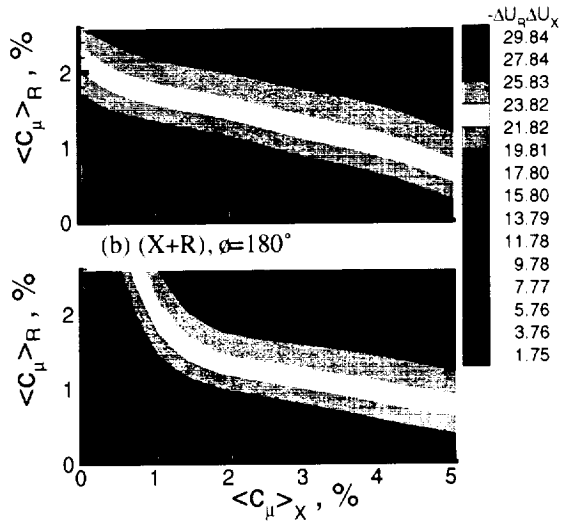

Figure 9a-b: Contours of change in shear-layer velocity at $z_{0.5,b}$ due to excitation at x/D=2.5, and $Re_D=3.1x10^4$.

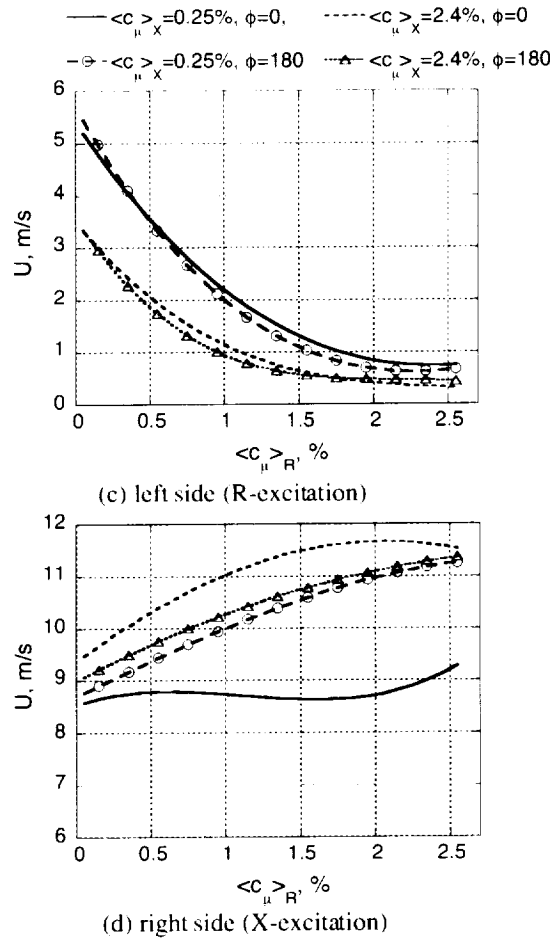

Figure 9c-d: Shear-layer velocity changes at $z_{0.5,b}$ due to (X+R) excitation at x/D=2.5 and $Re_D=3.1x10^4$.

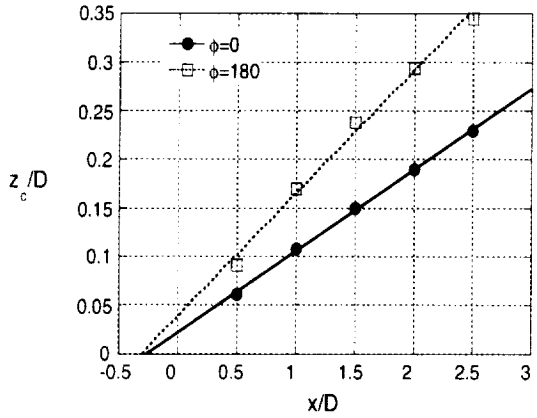

Figure 10: Streamwise variation of jet center of linear momentum. $F^+=4.2$, $\langle c_\mu \rangle_X=0.14\%$, and $\langle c_\mu \rangle_R=1.76\%$

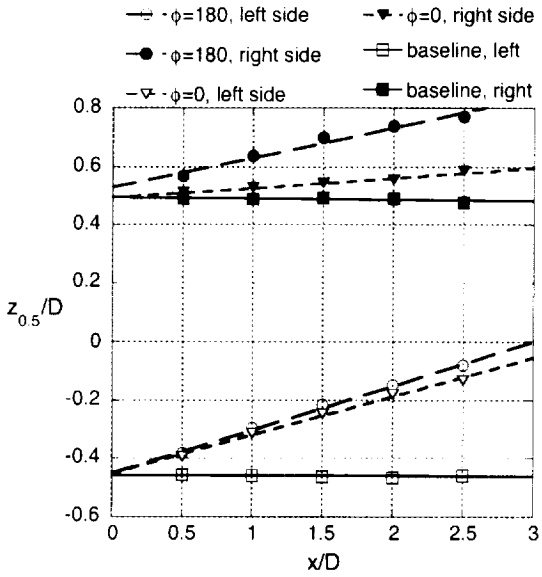

Figure 11: Variation of $z_{0.5}$ with x/D. $Re_D=3.1\times10^4$, $F^+=4.2$, $\langle c_\mu \rangle_X=0.14\%$, $\langle c_\mu \rangle_R=1.76\%$

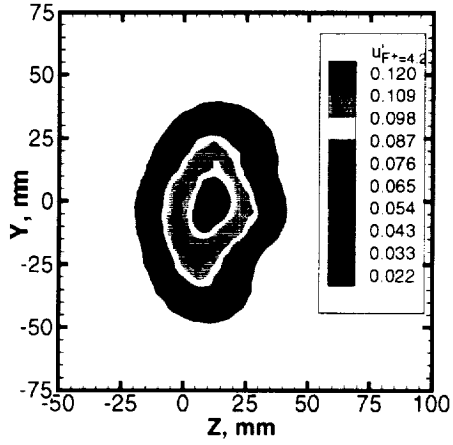

Figure 12a: Contours of amplitude of u' using (X+R), ø=0 excitation with $F^+=4.2$, $\langle c_\mu \rangle_X=0.58\%$, $\langle c_\mu \rangle_R=1.5\%$, $Re_D=3.1\times10^4$, and x/D=2.5.

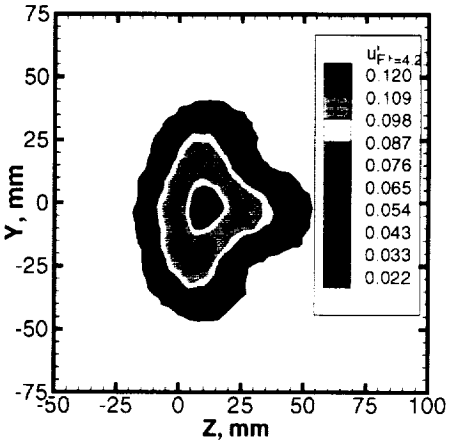

Figure 12b: Contours of amplitude of u' using (X+R), ø=180° excitation with $F^+=4.2$, $\langle c_\mu \rangle_X=0.58\%$, $\langle c_\mu \rangle_R=1.5\%$, $Re_D=3.1\times10^4$, and x/D=2.5.

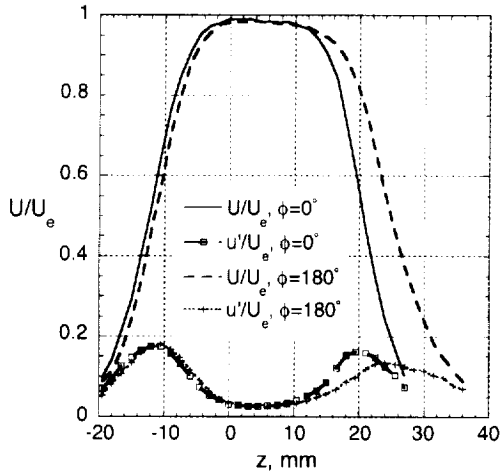

Figure 13a: Mean Velocity profiles at x/D=1.0. $F^+=4.2$, $\langle c_\mu \rangle_X=0.14\%$, and $\langle c_\mu \rangle_R=1.76\%$

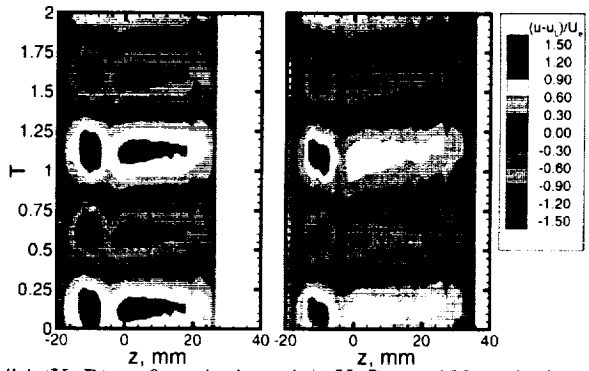

(b) (X+R), ø=0 excitation (c) (X+R), ø=180 excitation

Figure 13b-c: Contours of phase-locked velocity fluctuations over two cycles. $F^+=4.2$, $\langle c_\mu \rangle_X=0.14\%$, $\langle c_\mu \rangle_R=1.76\%$, x/D=1.0, $Re_D=3.1\times10^4$.

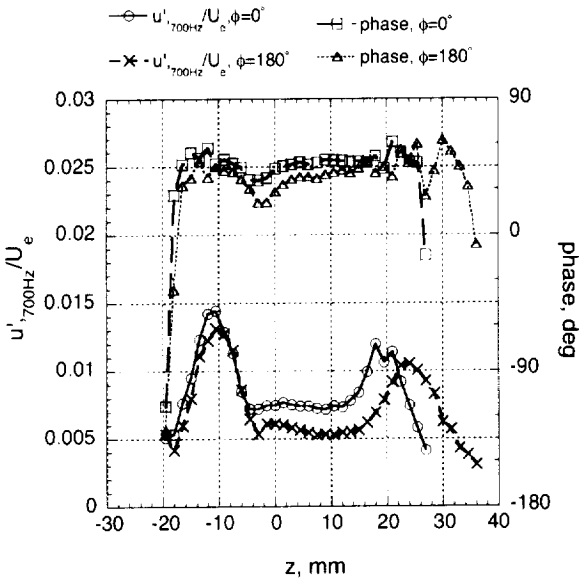

Figure 13d: Velocity fluctuations, u', at F^{+}=4.2 and phase angle, $\langle c_\mu \rangle_X$=0.14%, $\langle c_\mu \rangle_R$=1.76%, x/D=1.0, and Re_D=3.1x10^4.